Olivary Particles: Unique Carbon Microstructure Synthesized by Catalytic Pyrolysis of Acetone

Tao Luo, Lisheng Gao, Jianwei Liu, Luyang Chen, Jianmin Shen, Licheng Wang, and Yitai Qian*

Hefei National Laboratory for Physical Sciences at Microscale and Department of Chemistry, University of Science and Technology of China, Hefei, 230026, People's Republic of China

Received: April 6, 2005; In Final Form: May 27, 2005

Olivary (olive-shaped) carbon particles (OCPs) with a diameter of ∼1.5−2 μm at the middle and a length of ∼3−4 μm were synthesized by pyrolysis of acetone with metallic zinc as the catalyst at 600 °C. The content of the OCPs in the product is related to the catalyst, the pyrolysis temperature, and the time of ultrasonic dispersion before pyrolysis. The content of the OCPs was over 90% of the product under the optimum condition. Mg, Ni, Fe, Cu, Zn, and Cd powder were used as catalysts in the experiments, respectively, in which the metallic zinc powder was outstanding in the pyrolyzing process; the metallic iron and cadmium powder also improved the formation of the olivary carbon particles; however, magnesium, nickel, and copper could not operate the catalysis. Through Fourier transform infrared spectroscopy analysis, the mechanism of the formation of the olivary carbon particles was suggested to be an indirectly catalytic and self-assemble process. By high-resolution transmission electron microscope observation, an interesting arrangement of crystal planes of carbon was found that (002) planes of graphite near the surface are vertical to the surface of the OCPs and not parallel as usual.

Introduction

The discovery of the carbon nanotubes[1] stimulated intense interest in the structures accessible to carbon. In recent years, considerable efforts have been made to fabricate carbon materials with different forms and explore their applications.[2−10] The graphitic cones were synthesized by the pyrolysis of hydrocarbon in a carbon arc.[11] The hollow carbon cones have been synthesized by reduction of butyl alcohol with metallic magnesium at 500 °C.[12] Hollow carbon spheres[13,14] and carbon onions[15−17] were also successfully synthesized.

More recently, a few core−shell particle and hollow capsules have been synthesized using carbon spheres as templates.[18−20] Up to now, few works have been reported about nonspherical core−shell particles and hollow capsules due to the lack of nonspherical templates. However, nonspherical templates may be more attractive in applications than their spherical counterparts because of their low symmetries. And it is worth finding methods to synthesize nonspherical carbon particles as new templates.

Herein, we reported a catalytic pyrolysis approach to synthesize olivary carbon particles in autoclave at 600 °C. To the best of our acknowledge, it is the first time olive-shaped carbon material has been prepared. The time of ultrasonic dispersion, the catalyst, and the temperature of pyrolysis we adopted were investigated.

Experimental Section

In a typical experiment, 1.0 g of metallic zinc powder (99%) and 10.5 mL of acetone were mixed and ultrasonicated for 30 min and then put into a 15-mL stainless steel autoclave. After being sealed, the autoclave was heated from room temperature to 600 °C (10 °C/min) and maintained at 600 °C for 12 h and then cooled to room temperature naturally. The product was collected and washed by pure ethanol, dilute hydrochloric acid, and distilled water several times. After that, the product was dried in a vacuum at 60 °C for 6 h. About 1.3 g of final product was obtained.

The X-ray diffraction (XRD) analysis was performed on a Philips X'Pert PROSUPER X-ray powder diffractometer (Cu Kα radiation $\lambda = 1.541874$ Å). The morphologies of the samples were further characterized with scanning electron microscopy (SEM, JEOL JSM-6700F). The high-resolution transmission electron microscopy (HRTEM) images and the corresponding electron diffraction (ED) patterns were taken on a JEOL 2010 high-resolution transmission electron microscope performed at an acceleration voltage of 200 kV. The Raman spectrum was recorded at ambient temperature on a LABRAM-HR confocal laser MicroRaman spectrometer with an argon-ion laser at an excitation wavelength of 514.5 nm. Fourier transform infrared (FTIR) spectra were recorded on an EQUINOX 55 Fourier transmission IR spectrometer.

Result and Discussion

All the reflection peaks of the product (shown in Figure 1a) can be indexed to hexagonal graphite (JCPDS card file, no. 75-1621), hexagonal zinc oxide (JCPDS card file, no. 75-0576), and unreacted zinc (JCPDS card file, no. 04-0831). Figure 1b is the XRD pattern of the products washed by dilute HCl aqueous solution and distilled water, which can be indexed to graphite.

* To whom correspondence should be addressed. Fax: 86 551 3631760. E-mail: ytqian@ustc.edu.cn.

10.1021/jp051781z CCC: $30.25
Published on Web 07/26/2005

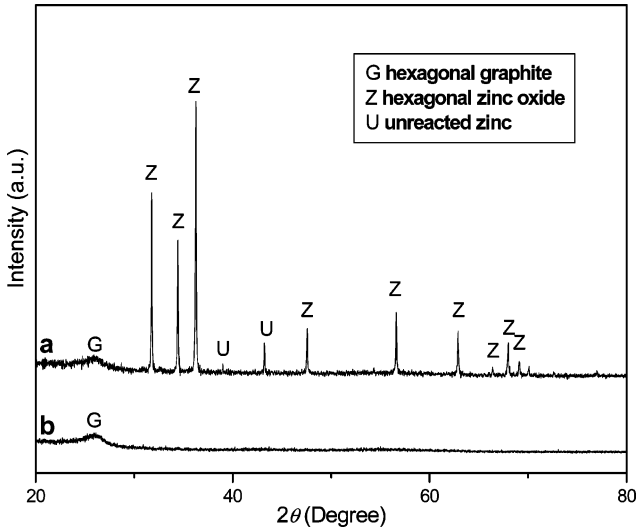

Figure 1. XRD patterns of the products with different treatments: (a) not washed; (b) washed with dilute HCl aqueous solution and distilled water.

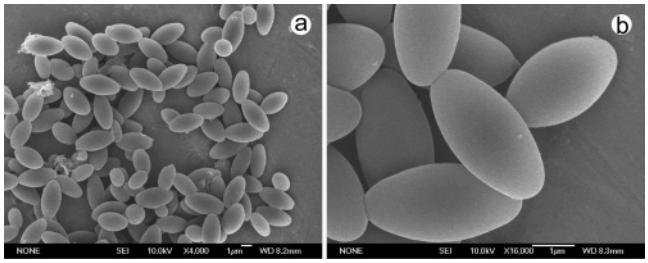

Figure 2. SEM images of the as-prepared products.

The SEM image in Figure 2a shows uniform olivary morphology of the as-obtained carbon particles and indicates that the as-obtained sample is homogeneous in shape. It can be seen in Figure 2b that the olivary carbon particles with a diameter of ~1.5−2 μm at the middle and a length of ~3−4 μm have smooth surfaces. Through SEM observation, the content of the olivary carbon particles (OCPs) was estimated over 90% of the product. The HRTEM image (in Figure 3a) shows an interesting phenomenon that (002) planes of graphite near the surface are vertical to the surface of the OCPs not parallel as usual. Parts c and d of Figure 3 show the selected-area electron diffraction (SAED) patterns of points 1 and 2 in Figure 3b. From them, we can observe that the lines linking the two midpoints of a pair of (002) arcs parallel with the tangent lines through the points 1 and 2 in Figure 3b, respectively, which also confirms the unusual arrangement of crystal planes of carbon. The HRTEM image indicates that there are many defects and disorders in the (002) planes and a layer of amorphous carbon on the surface of the OCP, which agrees with the abroad (002) peak in the XRD diagram.

The representative Raman spectrum of the sample (Figure 4) shows that there are two strong peaks at 1345 and 1594 cm^{-1}.

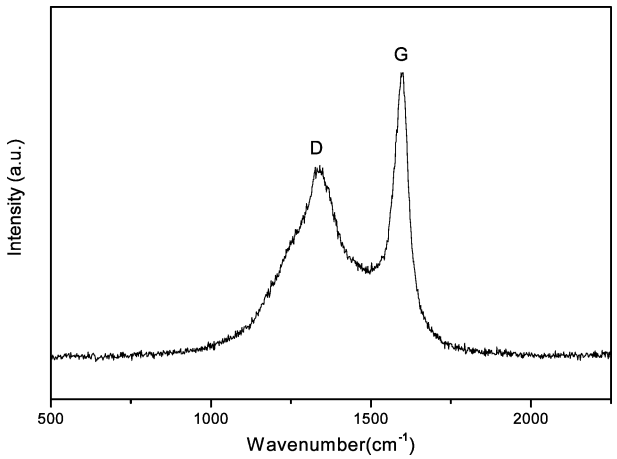

Figure 4. Raman spectrum of the as-prepared sample.

The peak at 1594 cm^{-1} (G-bond) corresponding to the Raman-allowed optical mode E_{2g} of 2-dimensional graphite is closely related to the vibration in all sp^2 bonded carbon atoms in a 2-dimensional hexagonal lattice, such as in a graphene layer. The peak at 1345 cm^{-1} could be assigned to the vibrations of carbon atoms with dangling bonds in planar terminations of disordered graphite.[21] The Raman spectrum clearly shows that the sample is highly disordered, in agreement with XRD pattern and TEM observation.

The effect of the ultrasonic dispersion time on the formation of the OCPs was investigated. Parts a−c of Figure 5 shows the SEM images of the as-obtained products through 5-, 10-, and 20-min ultrasonic dispersion before the pyrolysis at 600 °C, respectively. With the time of the ultrasonic dispersion increasing, the sizes of the OCPs tend to become even and the content of the OCPs in the products increase. When the time of the ultrasonic dispersion was prolonged to 30 min, the morphology of the OCPs became uniform and most of the products were the OCPs (shown in Figure 2a). A further study on the ultrasonic dispersion was carried out using FTIR spectroscopy. Figure 6 shows the FTIR spectra of the acetone after 0, 5, 10, 20, 30 min of ultrasonic dispersion. The absorption peak at the wavenumber ν (~3005 cm^{-1}) corresponding to the C−H stretching vibration of =C−H enlarges gradually with increasing the ultrasonic dispersion time, which indicates that the ultrasonication prompts acetone molecule to transform from ketone form to enol form−2-allyl alcohol. From the above results, it is reasonable to conclude that 2-allyl alcohol plays a crucial role in the formation of the OCPs.

The temperature of the reaction was an important factor in the formation of the OCPs. When the temperature was below 500 °C, there was no carbon in the product. Contrarily, the

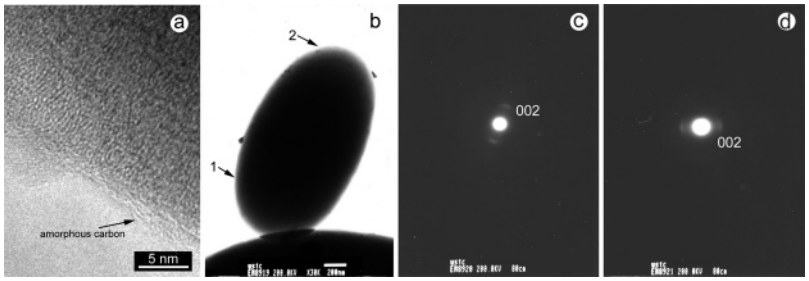

Figure 3. (a) HRTEM image showing the border of the OCP; (b) TEM image of the product; (c) SAED image of point 1 in (b); (d) SAED image of point 2 in (b).

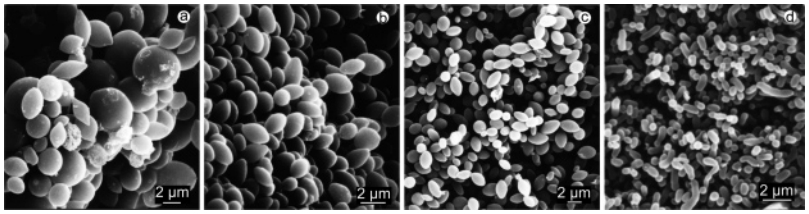

Figure 5. SEM images of as-obtained samples by different time of the ultrasonic dispersion before pyrolysis of acetone at 600 °C: (a) 5 min; (b) 10 min; (c) 20 min. (d) By pyrolysis of acetone with zinc at 700 °C after 30 min of ultrasonic dispersion.

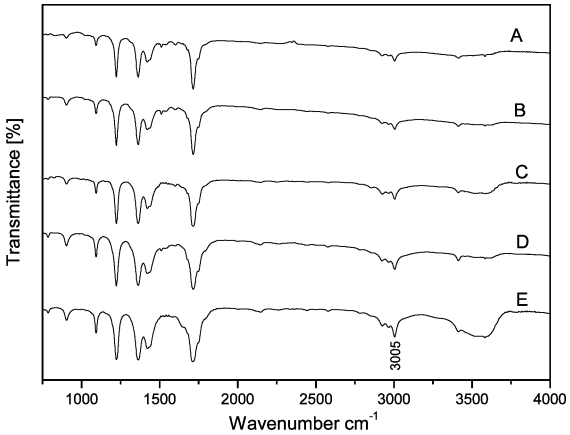

Figure 6. FTIR spectra of acetone with different ultrasonic dispersion times: A, 0 min; B, 5 min; C, 10 min; D, 20 min; E, 30 min.

olivary particles conglutinated to form carbon fibers at the temperature of 700 °C (shown in Figure 5d). From the above experiments, 600 °C was considered the optimum temperature of the pyrolysis to form the OCPs.

To investigate the mechanism of the pyrolysis process, three samples with different conditions were studied via FTIR spectroscopy. Figure 7 shows the FTIR spectra of (A) the reactant acetone; (B) the products by pyrolysis of the reactant acetone at 400 °C without the catalyst; (C) the products by pyrolysis of the reactant acetone at 400 °C with the metallic zinc powder as the catalyst; (D) the products by pyrolysis of the reactant acetone at 600 °C with the metallic zinc powder as the catalyst; (E) the products by pyrolysis of the reactant acetone at 600 °C without the catalyst. By comparison of part A with part B of Figure 7, it can be found that the acetone is unchanged at 400 °C with the absence of the catalyst. Figure 7D as well as Figure 7E indicated that there was no hydrogen in the final product. In Figure 7C, three absorption bands around the wavenumber ν ($\sim$2957 cm^{-1}) correspond to the asymmetrical and symmetrical C−H stretching vibration of $-CH_3$. The wavenumber ν ($\sim$1450) belongs to the C−H scissoring vibration of $-CH_2-$. The wavenumber ν ($\sim$1366) is generated by the OH bending vibration of tertiary aliphatic alcohols. There are two points presented by the result of the IR spectroscopy: (1) the 2-allyl alcohol polymerized; (2) the catalyst played an important role in the polyreaction. The formula can be schematized as follows

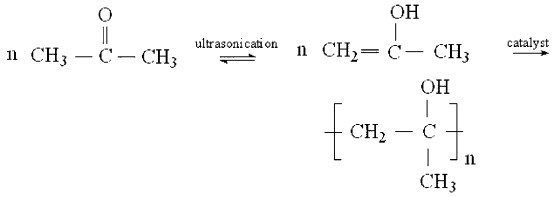

From the above experiments, the growth mechanism of the OCPs can be suggested as a mediate catalyze and self-assemble process. The catalysts do not operate on the formation of the olivary-like morphology directly but operate on the polyreaction

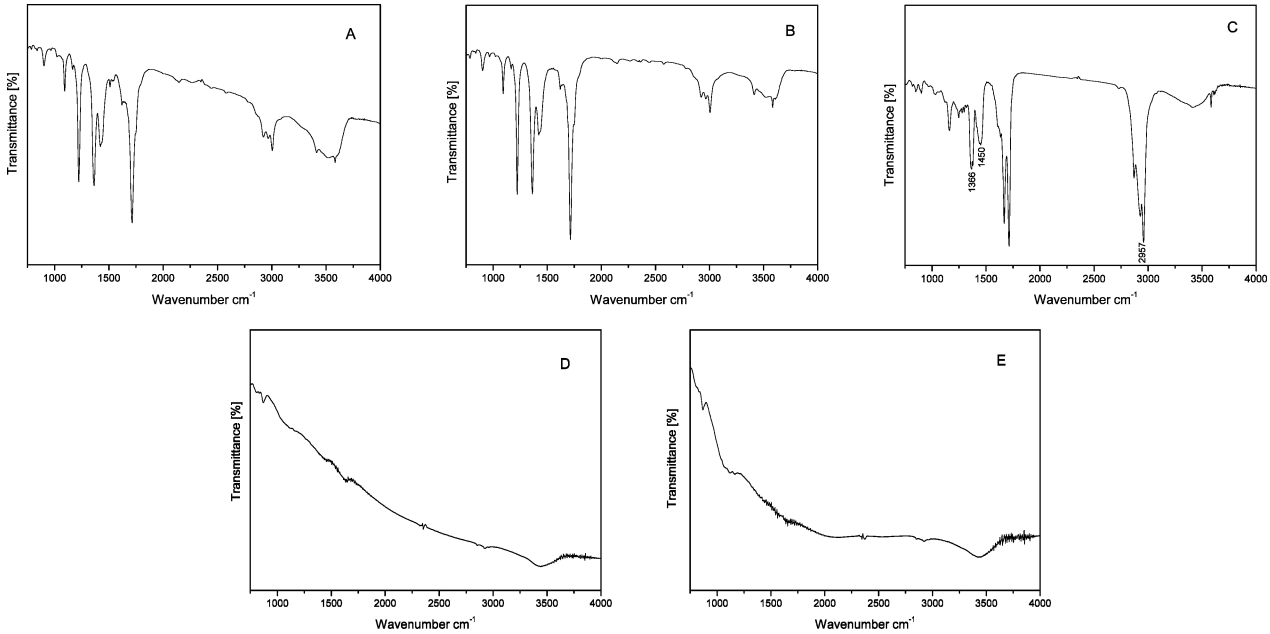

Figure 7. (A) FTIR spectrum of the reactant acetone; (B) FTIR spectrum of the product by pyrolysis of the reactant acetone at 400 °C without the catalyst; (C) FTIR spectrum of the product by pyrolysis of the reactant acetone at 400 °C with the metallic zinc powder as the catalyst; (D) FTIR spectrum of the product by pyrolysis of the reactant acetone at 600 °C with the metallic zinc powder as the catalyst; (E) FTIR spectrum of the product by pyrolysis of the reactant acetone at 600 °C without the catalyst (the reactant acetone via 30 min of sonication).

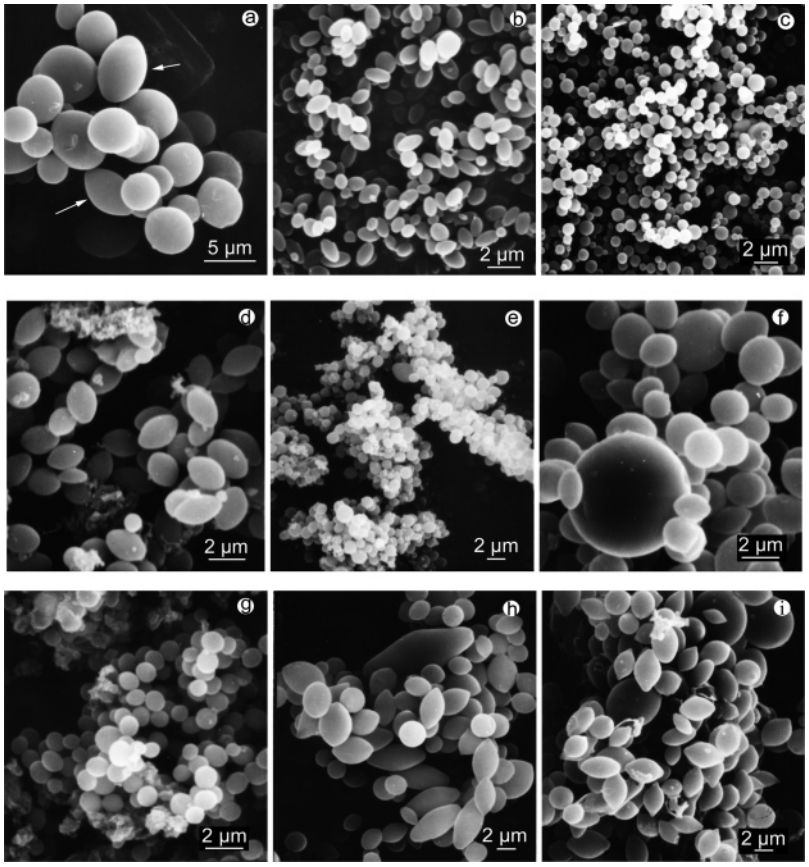

Figure 8. SEM images of the samples obtained by pyrolysis of acetone at 600 °C with different powders: (a) with no powder; (b) with zinc powder; (c) with magnesium powder; (d) with magnesium and zinc powder; (e) with magnesium and zinc oxide powder; (f) with copper powder; (g) with nickel powder; (h) with iron powder; (i) with cadmium powder. (Ultrasonic dispersion (30 min) had been carried out before pyrolysis in the above all experiments.)

to form the intermediate products, which form the olivary carbon particles by self-assembly in the pyrolysis process. The content of the enol form in acetone was very low due to its instability. Through 30 min of ultrasonication, the ratio of the 2-allyl alcohol increased. With the catalyst, the 2-allyl alcohol polymerized gradually with the temperature increasing to form the intermediate product, which was a kind of polyhydroxy alcohol with a carbon chain. And the conformations of intermediate product most probably directly play an important role in the pyrolysis process. The carbon chain and the multihydroxy of the intermediate product may operate the directional function in the intermolecular dehydration process, which make a preferential growth orientation in the pyrolysis process. So the products were the olivary particles with long axes, which are most probably related to the long carbon chains. When the temperature of the pyrolysis was at 700 °C, the preferential growth orientation was shown clearly by the carbon fibers in Figure 5d.

To select the effective catalyst, further experiments were carried out. Figure 8a shows the SEM image of the sample by pyrolysis of acetone without catalysts. Some olivary particles can be seen in Figure 8a, which indicates that acetone has a self-orientation to form olivary morphology in the process of pyrolysis. When the metallic zinc powder was added in the autoclave, the morphology and the content of the olivary particles in the product were both improved (shown in Figure 8b). When the metallic magnesium powder replaced zinc, no improvement in the formation of the product could be found in Figure 8c. To determine if metallic zinc or zinc oxide performed a catalytic function, two contrasting experiments were executed. One was pyrolysis of 10.5 mL of acetone with 0.523 g of magnesium and 0.065 g of zinc at 600 °C, and the SEM image of the product was shown in Figure 8d. The other was pyrolysis of 10.5 mL of acetone with 0.523 g of magnesium and 0.081 g of zinc oxide at 600 °C, and the SEM image of the product was shown in Figure 8e. We could not find the improvement in the morphology and the content of the product in Figure 8e as in Figure 8d. The above two experiments indicated that the metallic zinc operated as a catalyst in the reaction. The metallic powders of copper, nickel, iron, and cadmium were used instead of zinc, respectively, with other experiment conditions unchanged. Parts f−i of Figure 8 show the SEM images of these products, respectively, which indicates that metallic copper and nickel powder cannot catalyze the formation of olivary carbon particles, while metallic cadmium and iron powder can partially improve the formation of the OCPs but cannot parallel with metallic zinc powder. Figure 9 shows the XRD patterns of the products without washed with dilute hydrochloric acid by different catalysts: (A) magnesium; (B) nickel; (C) iron; (D) copper; (E) cadmium. The XRD pattern in Figure 9A can be indexed to graphite, magnesium oxide (JCPDS card file, no. 45-0946), and magnesium carbonate (JCPDS card file, no. 86-0175). In Figure 9B: graphite and nickel (JCPDS card file, no. 04-0850). In Figure 9C: graphite and magnetic iron oxide (JCPDS card file, no. 85-1436). In Figure 9D: graphite and copper (JCPDS card file, no. 04-0836). In Figure 9E: graphite, cadmium (JCPDS card file, no. 05-0674), and cadmium carbonate (JCPDS card file, no. 42-1342). Through analysis of the XRD pattern of the products, it could be found that cadmium, iron, and zinc had reacted with acetone in the experiments but that copper and nickel had not. The most reasonable explanation is proposed that the metallic cadmium, iron, and zinc powders

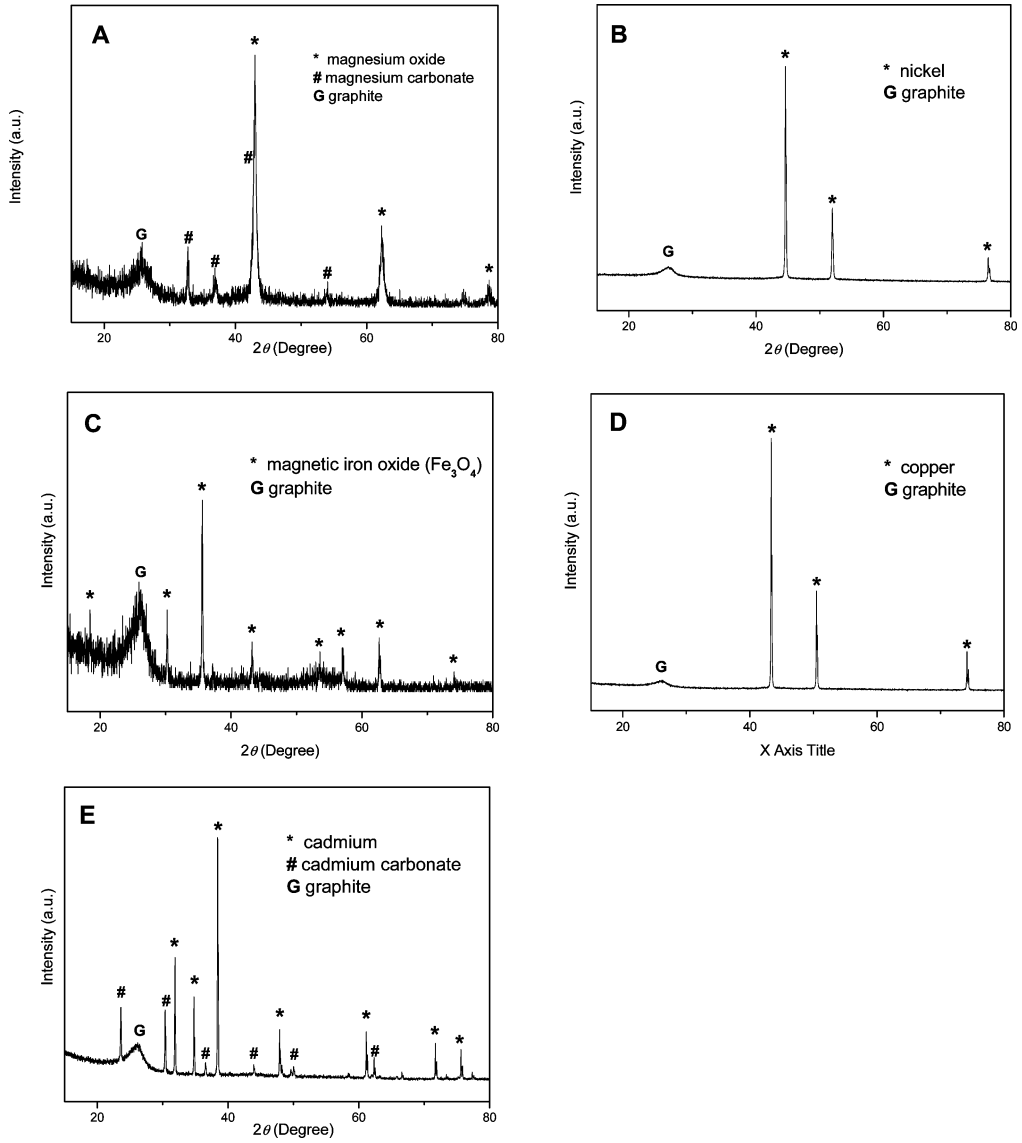

Figure 9. XRD patterns of the products by different catalysts: (A) magnesium; (B) nickel; (C) iron; (D) copper; (E) cadmium.

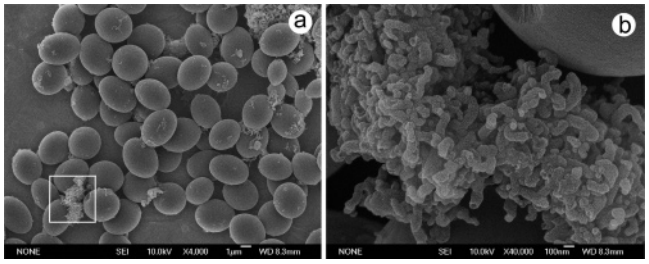

Figure 10. (a) FESEM image of the products by butanone instead of acetone; (b) FESEM image of the square in (a) under higher magnification.

react with acetone to trigger the polyreaction. Although magnesium can react with acetone, it is not an effective catalyst. As known, magnesium is more active than cadmium, iron, and zinc. So it is proposed that magnesium reacted with acetone too strongly and quickly to give enough time for the chain growth in the polymerization process.

To prove the feasibility of the proposed mechanism, acetone was replaced by the homologous compound butanone. The OCPs were also obtained with a few carbon nanotubes (shown in Figure 10).

Conclusion

In summary, unique carbon microstructures with the olivary particles were synthesized by the catalytic pyrolysis of acetone in an autoclave at 600 °C. The parameters of the experiment were studied such as the time of ultrasonic dispersion and the pyrolyzing temperature. The enol form of acetone played a crucial role in the formation of the OCPs. With concern for the catalyst, the metallic zinc powder was superior to the others in the pyrolyzing process; the metallic iron and cadmium powder could also improve the formation of the olivary carbon particles; however, magnesium, nickel, and copper powder could not operate the catalysis. The catalyst controlled the formation of the OCPs via catalyzing the polyreaction to form the intermediate. This mediated-catalysis mode has potential applications in other catalytic synthesis processes. The OCPs not only can be used as templates for synthesis other materials but also have potential applications in gas storage media, catalyst carrier, and structure composite due to their unique arrangement of (002) planes of carbon near the surface.

Acknowledgment. This work is supported by the National Natural Science Foundation of China and 973 Projects of China.

References and Notes

(1) Lijima, S. *Nature* **1991**, *354*, 56.
(2) Kyotani, T.; Tsai, L. F.; Tomita, A. *Chem. Mater.* **1996**, *8*, 2109.
(3) Benito, A. M.; Maniette, Y.; Munoz, E.; Martinez, M. T. *Carbon* **1998**, *36*, 681.
(4) Kim, P.; Lieber, C. M. *Science* **1999**, *286*, 2148.
(5) Fan, S. S.; Chapline, M. G.; Franklin, N. R.; Tombler, T. W.; Cassell, A. M.; Dai, H. J. *Science* **1999**, *283*, 512.
(6) Zhu, H. W.; Xu, C. L.; Wu, D. H.; Wei, B. Q.; Vajtai, R.; Ajayan, P. M. *Science* **2002**, *296*, 884.
(7) Alekseyev, N. I.; Dyuzhev, G. A. *Carbon* **2003**, *41*, 1343.
(8) Frank, S.; Poncharal, P.; Wang, Z. L.; de Heer, W. A. *Science* **1998**, *280*, 1744.
(9) Liu, C.; Fan, Y. Y.; Liu, M.; Cong, H. T.; Cheng, H. M.; Dresselhaus, M. S. *Science* **1999**, *286*, 1127.
(10) Liu, J. W.; Shao, M. W.; Chen, X. Y.; Yu, W. C.; Liu, X. M.; Qian, Y. T. *J. Am. Chem. Soc.* **2003**, *125*, 8088.
(11) Krishnan, A.; Dujardin, E.; Treacy, M. M. J.; Hugdahl, J.; Lynum, S.; Ebbesen, T. W. *Nature* **1997**, *388*, 451.
(12) Liu, J. W.; Lin, W. J.; Chen, X. Y.; Zhang, S. Y.; Li, F. Q.; Qian, Y. T. *Carbon* **2004**, *42*, 667.
(13) Hu, G.; Ma, D.; Cheng, M. J.; Liu, L.; Bao, X. H. *Chem. Commun.* **2002**, 1948.
(14) Liu, J. W.; Shao, M. W.; Tang, Q.; Chen, X. Y.; Liu, Z. P.; Qian, Y. T. *Carbon* **2002**, *411*, 1682.
(15) Cabioc'h, T.; Thune, E.; Jaouen, M. *Chem. Phys. Lett.* **2000**, *320*, 202.
(16) Chen, X. H.; Deng, F. M.; Wang, J. X.; Yang, H. S.; Wu, G. T.; Zhang, X. B.; Peng, J. C.; Li, W. Z. *Chem. Phys. Lett.* **2001**, *336*, 201.
(17) Nasibulin, A. G.; Moisala, A.; Brown, D. P.; Kauppinen, E. I. *Carbon* **2003**, *41*, 2711.
(18) Sun, X. M.; Li, Y. D. *Angew. Chem.* **2004**, *43*, 597.
(19) Li, X. L.; Lou, T. J.; Sun, X. M.; Li, Y. D. *Inorg. Chem.* **2004**, *43*, 5442.
(20) Sun, X. M.; Li, Y. D. *Angew. Chem.* **2004**, *43*, 3827.
(21) Barbarossa, V.; Galluzzi, F.; Tomaciello, R.; Zanobi, A. *Chem. Phys. Lett.* **1991**, *185*, 53.